

A Novel Noninvasive Technique for Pulse-Wave Imaging and Characterization of Clinically-Significant Vascular Mechanical Properties *In Vivo*

KANA FUJIKURA,¹ JIANWEN LUO,¹ VIKTOR GAMARNIK,¹ MATHIEU PERNOT,¹
ROYD FUKUMOTO,² MARTIN DAVID TILSON III^{2,3} AND ELISA E. KONOFAGOU^{1,4}

¹*Department of Biomedical Engineering
Columbia University
1210 Amsterdam Avenue
New York, NY 10027
ek2191@columbia.edu*

²*St. Luke's-Roosevelt Hospital Center
New York, NY*

³*Department of Surgery
Columbia University, New York, NY 10027*

⁴*Department of Radiology
Columbia University, New York, NY 10027*

The pulse-wave velocity (PWV) has been used as an indicator of vascular stiffness, which can be an early predictor of cardiovascular mortality. A noninvasive, easily applicable method for detecting the *regional* pulse wave (PW) may contribute as a future modality for risk assessment. The purpose of this study was to demonstrate the feasibility and reproducibility of PW imaging (PWI) during propagation along the abdominal aortic wall by acquiring electrocardiography-gated (ECG-gated) radiofrequency (rf) signals noninvasively. An abdominal aortic aneurysm (AAA) was induced using a CaCl₂ model in order to investigate the utility of this novel method for detecting disease. The abdominal aortas of twelve normal and five CaCl₂ mice were scanned at 30 MHz and electrocardiography (ECG) was acquired simultaneously. The radial wall velocities were mapped with 8000 frames/s. Propagation of the PW was demonstrated in a color-coded ciné-loop format in all cases. In the normal mice, the wave propagated in linear fashion from a proximal to a distal region. However, in CaCl₂ mice, multiple waves were initiated from several regions (i.e., most likely initiated from various calcified regions within the aortic wall). The *regional* PWV in normal aortas was 2.70 ± 0.54 m/s ($r^2 = 0.85 \pm 0.06$, $n = 12$), which was in agreement with previous reports using conventional techniques. Although there was no statistical difference in the *regional* PWV between the normal and CaCl₂-treated aortas (2.95 ± 0.90 m/s ($r^2 = 0.51 \pm 0.22$, $n = 5$)), the correlation coefficient was found to be significantly lower in the CaCl₂-treated aortas ($p < 0.01$). This state-of-the-art technique allows noninvasive mapping of vascular disease *in vivo*. In future clinical applications, it may contribute to the detection of early stages of cardiovascular disease, which may decrease mortality among high-risk patients.

Key words: Abdominal aortic aneurysm (AAA); wall velocity; radiofrequency (rf); *regional* pulse wave; ultrasound.

BACKGROUND

Aortic stiffness has been indicated as an early predictor of all-cause and cardiovascular mortality, primary coronary events, and fatal stroke.¹⁻⁶ In cases of aortic aneurysms, disrup-

tion of the medial elastic fibers may produce aortic stiffening, which may amplify the aneurysmal process.⁷ Pulse-wave velocity (PWV) has been shown capable of estimating the stiffness of arteries.⁸⁻¹⁰ Correlations of the aortic PWV and morphological changes associated with atherosclerosis have been previously reported.^{11, 12} Aging of the arterial system is accompanied by structural changes in the aortic wall, which leads to stiffening of the vasculature and increased velocity of the pressure wave as it travels down the aorta.¹³ The PWV in brachial arteries has also been proposed as a powerful independent indicator of all-cause mortality in diabetes¹⁴ and end-stage renal disease.¹⁵ As such, PWV measured along the aortic and aorto-femoral pathways is most clinically relevant because the aorta and its first branches are responsible for most of the pathophysiological effects of arterial stiffness and it has been indicated to be a strong predictor of future all-cause mortality.⁴ Although the diameter is currently used clinically as a predictor of rupture of the abdominal aortic aneurysm (AAA), increased compliance of the aneurysmal wall at the maximum diameter change over time has been discussed as a better rupture predictor. Noninvasive methods to evaluate the aortic wall of AAA have been investigated by several groups.¹⁶⁻¹⁹ MacSweeney et al¹⁶ used M-mode ultrasonography to demonstrate the marked stiffness or inelasticity of dilated or aneurysmal vessels, part of which has been attributed to the loss of elastin. Long et al^{17, 18} measured compliance of the abdominal aortic wall of AAA using tissue Doppler imaging and evaluated the relationship between the diameter of the aneurysm and the wall stiffness. These investigations demonstrated a significant increase in maximum mean segmental dilation and segmental compliance as well as a trend towards increased distensibility with increased diameter.^{17, 18} Jadhey and Kadam¹⁹ calculated the PWV in the human brachial artery using the time delay of PW recordings acquired from two different points. Truijers et al²⁰ evaluated asymptomatic, symptomatic and ruptured abdominal aortic aneurysm patients using computed tomography (CT), created a patient specific 3D model and calculated the wall stress using a finite-element method. Van de Geest et al²¹ calculated the wall strength from tensile testing of surgically-procured AAA wall specimens.

A noninvasive imaging method for detecting for *regional* PWV in the aorta may contribute to a future screening test to reduce the overall morbidity and mortality. Ultrasound allows noninvasive measurement of PWV and has been an area of recent interest.²²⁻²⁷ The PWV is defined as the distance between the two measurement points divided by the PW transit time-delay. Despite the simple definition of PWV, some problems still remain, which limit the interpretation of the available findings and the general applicability of the PWV measure.^{26, 28, 29} As pointed out recently, it has been very difficult to compare the values of PWV measurements from different research groups worldwide because of the lack of measurement standardization.²⁸ The accuracy of the PWV measured from two points suffers from errors of distance measurements and/or time-delay measurements. In addition, the reflected waves and noise from blood echoes may also affect these time-delay measurements. It is difficult to measure small time changes because the temporal resolution is low. Unusually, a large time change over a relative larger distance (a few cm) is needed for reliable measurements. Therefore, the PWV measured represents the average value between two measurement sites. In addition, the measurement of distance is based on the assumption that the arterial wall is unidimensional between two measurement points, which may not always hold.²⁹ A method with higher temporal and spatial resolution is needed in order to calculate the *regional* PWV. Recently, Zhang et al^{26, 30, 31} applied radiation force on the arterial wall *in vitro* to generate a propagating wave in the arterial wall phantom. The wave velocity was estimated from curve-fitting through several measurement points. Their temporal resolution was on the order of 1 μ s while the spatial resolution was on the order of 1 mm.

High-frequency ultrasound systems have recently become commercially available. To overcome limitations of frame rate in high-frequency systems, retrospective electrocardio-

gram (ECG) gating or prospective ECG triggering has been used.³²⁻³⁶ Using a high-resolution Vevo 770 system (VisualSonics Inc., Toronto, ON, Canada), Williams et al³⁷ evaluated the feasibility of measuring regional PWV using high-frequency ultrasound methodology by showing the similarity of PWVs derived by two image-guided approaches: a regional transit-time method and a local flow-area method. Our group recently developed an ultrafast radiofrequency (rf) data acquisition system based on the Vevo 770 system and the ECG gating technique.^{32,35} Rf data and ECG signals were acquired simultaneously and rf data corresponding to a complete cardiac cycle were then gated using the ECG to reconstruct the full-view two-dimensional (2D) images. The rf signals of the murine myocardium and aorta could be obtained at an extremely high frame rate (8000 frames/s or, 8 kHz), and Pernot et al^{32,35} were the first to visualize the PW propagation across the murine myocardium and along the abdominal aortic wall by colorizing displacement-velocity as a ciné-loop. The 2-D wall velocity maps at different times indicated mechanical wave propagation in the myocardium and aorta over a cardiac cycle.

As mentioned above, PWV is a surrogate measure of stiffness of the aortic wall, which may vary with the type and severity of disease. The purpose of this study was to visually display the velocity using color-coded ciné-loop. In the present experiments, the same methodology as in our previous study was used,^{32,35,36} including the Vevo 770 system, and the rf data and ECG acquisition protocol. The field of view was equal to 12 mm × 12 mm. The temporal resolution of our system was equal to 0.125 ms, i.e., the frame rate was equal to 8 kHz. The data were processed to display color-coded ciné-loop to allow us to visually identify and characterize the longitudinal wave propagation pattern. To our knowledge, this is the first time that feasibility of imaging the longitudinal *regional* PW propagation along the aortic wall itself is shown in a disease model. Throughout the entire paper, by *regional* PWV, we define the velocity of the wave imaged in the specific region of the aortic wall. This is in contrast with other studies that assign PWV measurements to the entire circulation.

We propose to use this technique for *regional* PW imaging (PWI) *in vivo*. We therefore hypothesize that the PWI technique that estimates and images wall velocity, *regional* PW propagation and wall elasticity is reproducible and that it may contribute to a novel, noninvasive modality of evaluating the mechanical properties of the aorta, both in the absence and presence of disease, qualitatively and quantitatively. We determined its capability of detecting these parameters of the abdominal aortic wall in mice using the extremely high frame-rate ultrasound system. The *regional* PW was imaged during propagation, the *regional* PWV was measured and the stiffness of the abdominal aortic wall was estimated by calculating its Young's modulus. The purpose of this study was thus to develop a reproducible technique and to demonstrate the feasibility of analyzing aortic wall mechanical properties noninvasively.

METHODS

Normal animal preparation

All procedures used in this study were approved by the institutional animal committee (IACUC) of Columbia University. Twelve wild-type C57BL/6 mice (three to four months old) were anesthetized with 125 mg/kg tribromoethanol (Sigma-Aldrich Corp., St. Louis, MO, USA), and the abdominal hair was removed using potassium thioglycolate. The mice were placed in the supine position on a heating platform (THM100, Indus Instruments, Houston, TX, USA) to maintain constant body temperature. ECG was obtained from the extremities. Figure 1A shows the positioning of the mice during data acquisition using the experimental set-up.

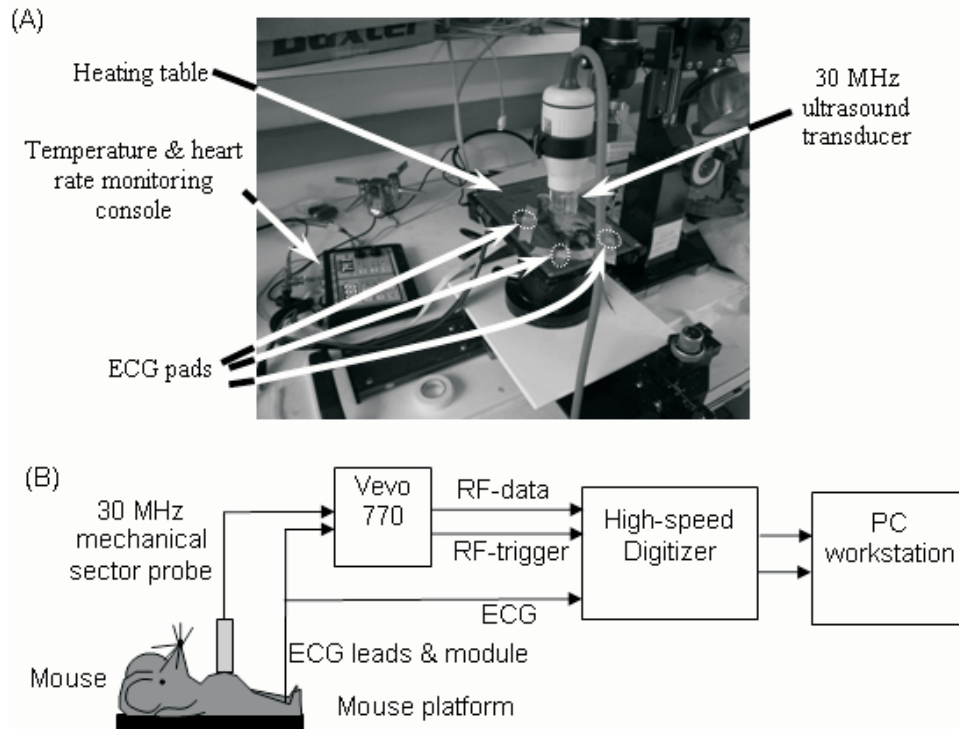


FIG. 1 A) Experimental *in-vivo* mouse setup for ultrasound data acquisition; B) Diagram of the different components in the experimental setup. Physiologic parameters (such as body temperature, heart rate) were simultaneously monitored in all experiments.

Ultrasound data acquisition and processing

A longitudinal view of the abdominal aorta was obtained noninvasively with ultrasound at 30 MHz with Vevo 770 system (VisualSonics Inc., Toronto, ON, Canada) using degassed ultrasound gel (Aquasonic 100, Parker Laboratories Inc., Fairfield, NJ, USA) as a coupling medium. The focal depth of the ultrasound transducer was 12.7 mm from the surface of the transducer, the field of view was 12 mm \times 12 mm, the axial resolution was equal to 55 μ m and the lateral resolution was equal to 115 μ m. The ultrasound probe was placed on the animal's abdomen in the parasternal position to obtain a longitudinal (long axis) view of the abdominal aorta in order to visualize the wave along the direction of propagation.

Figure 1B shows the data acquisition set-up. In the ECG-based kilohertz visualization (EKV) mode provided by VisualSonics Vevo 770 system, the transducer probe was mechanically moved in a section-scan format from one position to the other and ultrasound rf signals were recorded at a pulse repetition frequency (prf) of 8 kHz for each position of the probe. A two-channel, 160 MS/s, 14-bit Waveform Digitizer for Peripheral Component Interface (PCI) Bus (CompuScope 14200, Gage Applied Technologies, Inc., Lachine, QC, Canada) was used to synchronously acquire the rf signals of the ultrasound scanner and the associated ECG, with the ECG allowing gating of the rf signals. The data acquisition was triggered by the synchronization signal of the rf lines, which indicated when the transducer transmitted the ultrasound pulses.

After acquisition, the data was processed off-line on a Matlab-based software platform (Matlab 7.1, MathWorks, Inc., Natick, MA, USA) and the rf signals from different cardiac cycles were synchronized based on a standardized cardiac cycle, with adjusted R-R intervals

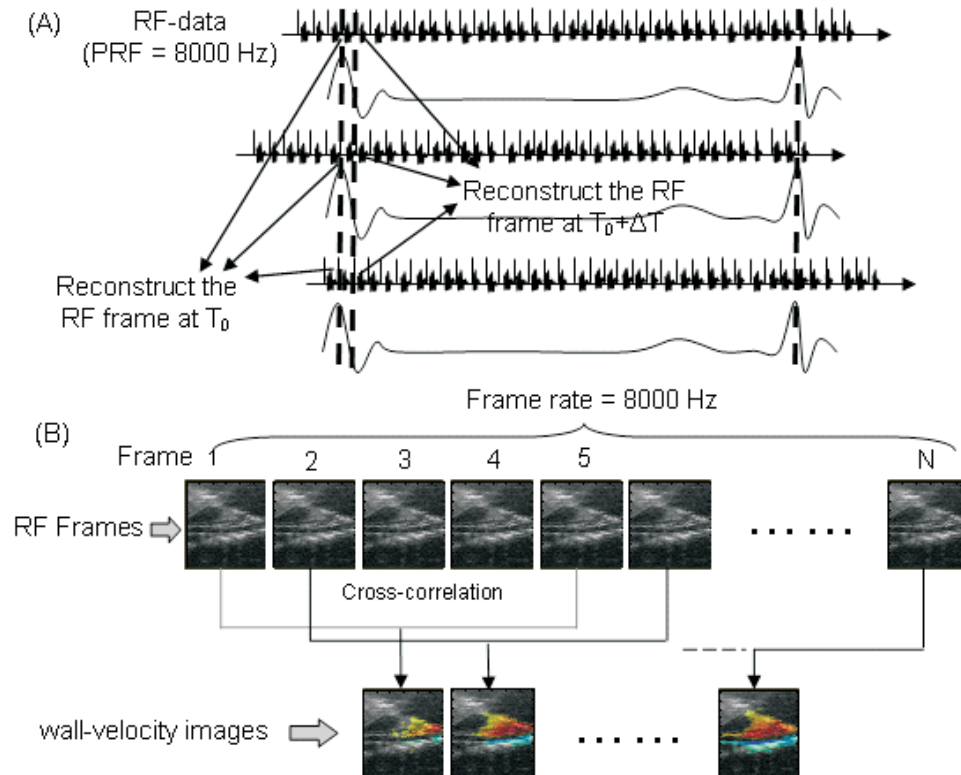


FIG. 2 A) rf line acquisition at multiple transducer locations (three examples are shown here): each line is synchronized relative to the R-wave (T_0); B) Multiple frame reconstruction from ECG-gated rf data. Reconstructed rf frames were acquired at a composite frame rate of 8,000 frames/s (fps) and analyzed with cross-correlation techniques to produce wall velocity images.

(Fig. 2A). With such a retrospective ECG-gating technique, the complete set of 2D ultrasound rf data was reconstructed at an extremely high frame rate of 8 kHz (i.e., equal to the pulse-repetition frequency) for a complete heart cycle.³² From the wall velocity distributions at different times, the PW in the abdominal aorta could be visualized. The velocity of the *regional* PW along the aortic wall was calculated as the slope of a linear regression fit.

Wall velocity estimation

The axial wall velocity was estimated off-line using a one-dimensional (1D) normalized cross-correlation technique on the rf signals acquired.^{38,39} The window size was equal to 240 μm with a 90% overlap in order to obtain the best tradeoff between precision of the estimate and resolution of the resulting image.

For each pair of consecutively acquired rf frames at 0.5 ms (or, 4 frames) apart in time (e.g. the i^{th} and $i+4^{\text{th}}$ frame in figure 2B), the radial displacement that occurred between the i^{th} to the $i+4^{\text{th}}$ frame, the $i+1^{\text{st}}$ to the $i+5^{\text{th}}$ frame, etc was imaged across the entire aortic segment imaged. The interval between the rf frames in each estimation pair was selected so as to yield the optimal wall velocity estimates, as previously reported.³⁶ By using this method, the effective frame rate for PWI was maintained at 8 kHz as in the ultrasound acquisition providing high temporal resolution, while the motion between two frames was large enough to provide high-quality estimation.³⁶ The wall velocities were color-coded and overlaid onto the grayscale 2D ultrasonic images (Figs. 3A-3D).

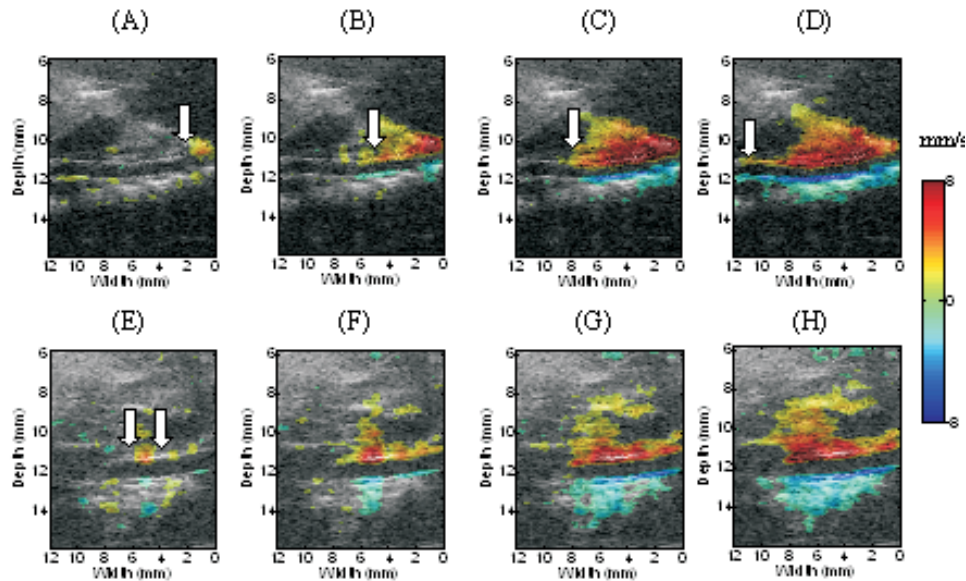


FIG. 3 Visualization of the propagation of the PW along the abdominal aortic wall, from the heart (right side of the images) to the renal arteries (left side of the images) in A-D) normal and E-H) CaCl_2 -model mice. Axial wall velocity maps (color maps) were overlaid onto the B-mode images for visualization. The time interval between sequential images corresponds to 1.25 ms between each depicted frame. Colors correspond to the axial wall velocity (mm/s) of the tissue. White arrows in (A-D) show the front of the wave as it propagates caudally along the dorsal and ventral aortic walls. The wavefront in (E-H) is harder to discern.

Regional PWV measurement

Using a 2D B-mode image, the anterior side of the aortic wall (i.e., near wall) was outlined between two manually-traced lines and the aortic wall was detected automatically as the maximum incremental/instantaneous wall velocity region between these two lines along each depth direction (FIG. 4A). The time of maximum wall velocity occurrence along the aortic wall segment delineated by the two lines in figure 4A was estimated. The distance from the proximal side of the aorta was plotted against the time of maximum wall velocity occurrence. Proximal denotes the segment closest to the heart (i.e., on the right side of each image shown) and distal denotes the segment farthest from the heart (i.e., on the left side of each image shown). The linear regression was performed to examine the relation between the distance and the timing of the maximum wall velocity and the slope was defined as indicative of the *regional* PWV. The correlation coefficient (r^2) was also calculated to evaluate the reliability of the *regional* PWV estimation. The results were expressed as mean \pm standard deviation (SD).

Young's modulus calculation

The theory of elastic wave propagation in soft biological tissues was considered in order to derive the Young's modulus of the aorta. Assuming that the medium is infinite and isotropic, the speed of shear wave propagation could simply be derived from general equations of the dynamic theory of elasticity.⁴⁰

For the transverse wave traveling along the arterial wall, a simple model of the propagation of a pressure wave in a viscoelastic infinite thin conduit filled with an incompressible fluid is well described by the Moens-Korteweg equation as follows:⁴¹

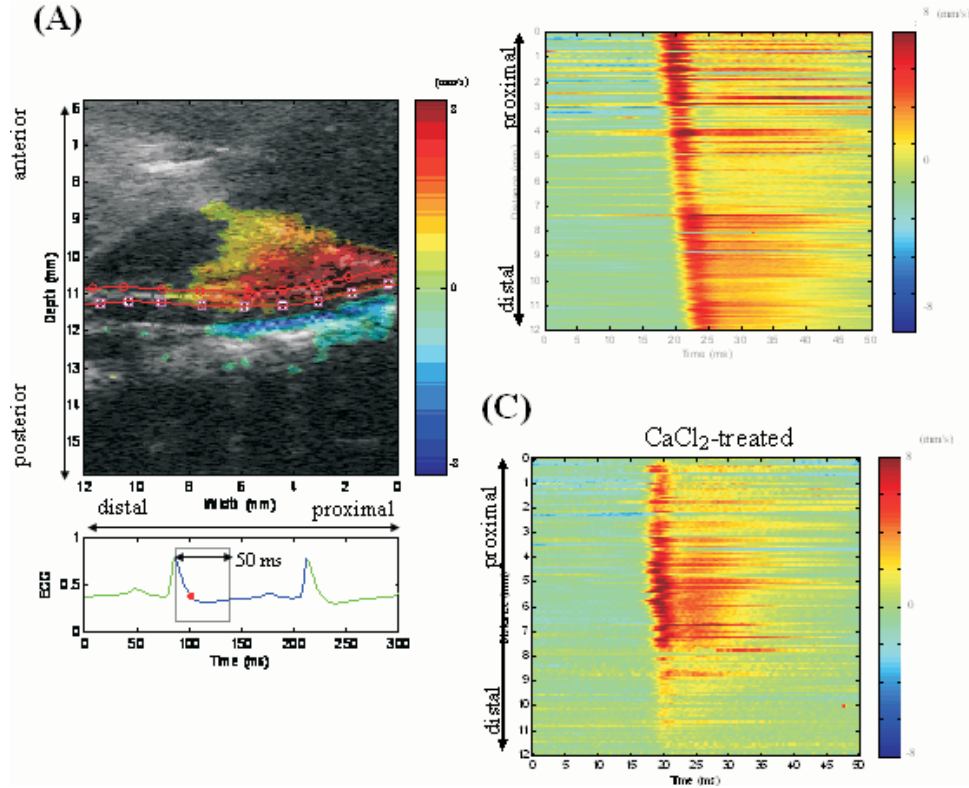


FIG. 4 A) PWI map and designation of two locations monitored with time in 2D spatiotemporal maps in B) normal and C) CaCl_2 -model murine aortas. Zero-point on horizontal axis corresponds to R-wave on ECG recording. Vertical axis corresponds to distance of maximum axial displacement from the rightmost side of the image acquired (heart side). Selection of the aortic wall for PWV analysis. The endothelial (\square) and epithelial (\circ) boundaries of the abdominal aorta were defined by the operator from a B-mode image.

$$c = \sqrt{\frac{Eh}{2R\rho}} \quad (1)$$

where c is the velocity, E is the Young's modulus of the conduit wall, h is the wall thickness, r is the density of the wall and R the inner radius of the aorta. The longitudinal Young's modulus was calculated, and the density of the aortic wall was assumed to be equal to 1060 kg/m^3 .⁴¹ According to this equation, the elasticity of the vascular wall can be derived from the measurement of the *regional* PWV in the vessel.

Wall velocity amplitude transition during one cardiac cycle

Two different segments on the aortic wall were tracked during one cardiac cycle to evaluate their variation of wall velocity amplitude across the wall. The wall velocity profiles were the average of five points composing $96 \mu\text{m}$ in depth. Those segments were on the rf lines located 3.6 mm and 7.2 mm from the proximal end of the full 2D image (Fig. 5A), and the wall velocity variation at those different distances is shown in figure 5B.

CaCl_2 animal model preparation

An AAA was induced by CaCl_2 to investigate the utility of this method for detecting disease. Five wild-type C57BL/6 mice, three to four months old, were anesthetized, and under-

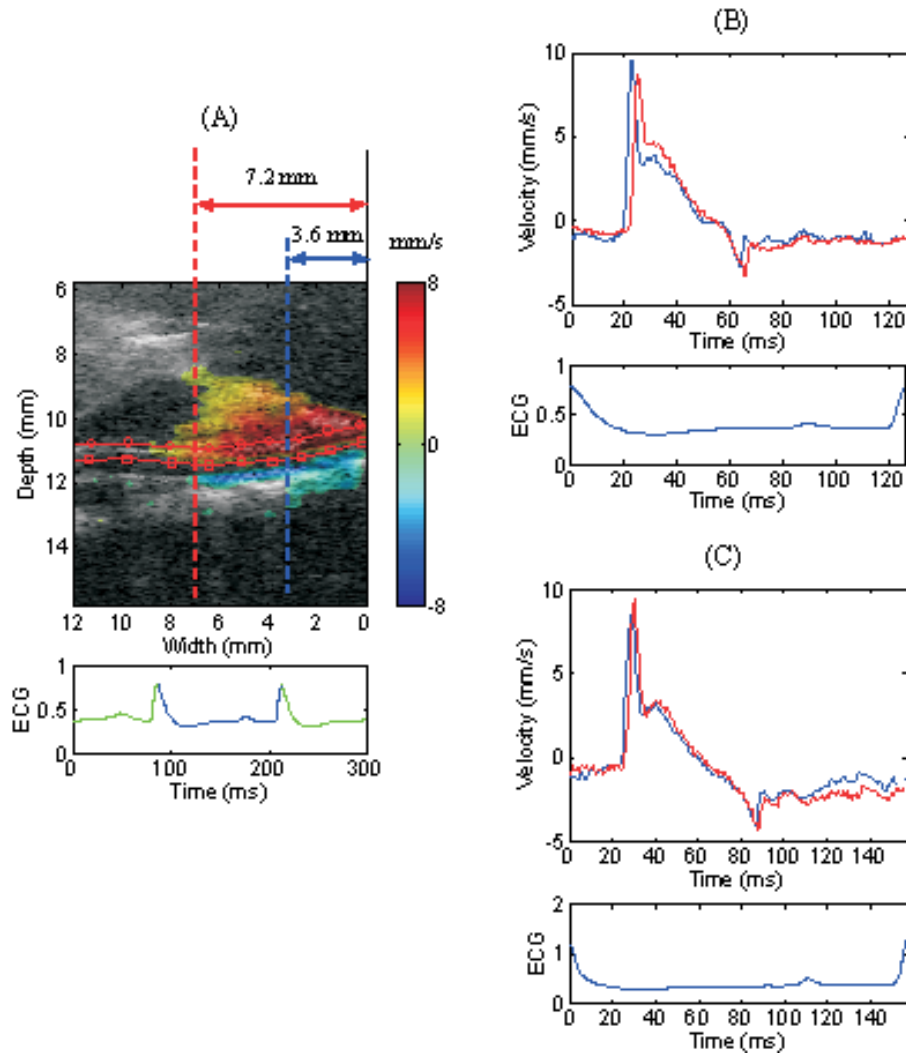


FIG. 5 A) Average displacement values were estimated on the abdominal aortic wall at 3.6 mm and 7.2 mm from the proximal side of the 2D image. B) Plots of displacements in two different locations in B) normal and C) CaCl_2 -model murine aortas. Selection of the optimal frame interval for displacement estimation was based on the graphs in B).

went laparotomy. The abdominal aortas of the mice were then exposed to 0.5 mol/L CaCl_2 as described in other studies.^{42, 43}

Four weeks after the operation, the abdominal aorta was scanned using the Vevo 770 system. The 2D (B-mode) images, rf data and ECG signals were simultaneously acquired. The diameter of the abdominal aortas was also measured using manual tracing on the B-mode to evaluate the aneurysm formation. Using the same methods as previously described, the wall velocity of the aortic wall was estimated and the sequential wave propagation was visually demonstrated. The results obtained from the normal and CaCl_2 mice were compared to evaluate the PWV change of the abdominal aortic wall caused by the disease.

Histopathology

The abdominal aorta of the normal and CaCl_2 mice were fixed in 10% formalin, and cut in paraffin blocks. Standard hematoxylin and eosin (H&E) and EVG staining was then performed.

RESULTS

The time course of the *regional* PW propagation was clearly visualized along the aortic wall by a color-coded ciné-loop with a frame rate of 8 kHz. Figures 3A-3D and 3E-3H display consecutive frames every 1.25 ms in normal and CaCl₂ aortas, respectively. In normal mice, the *regional* PW propagates from the proximal to the distal side with constant speed whereas in CaCl₂ aortas the wave was reflected at multiple locations.

The anterior side of the aortic wall (i.e., near wall) was delineated as shown in figure 4A and the aortic wall was automatically detected between those two lines, as described in the previous section. The time course of the aortic wall was tracked during one cardiac cycle for a period of 50 ms after the R-wave peak (Fig. 4B) as indicated in the ECG trace in figure 4A. The wall velocity variation for each rf line was displayed horizontally, along the entire abdominal aortic segment imaged, as shown in figures 4B and 4C. Figures 4B and 4C depict the propagation of the maximum wall velocity in the normal and CaCl₂ aortas, respectively. The top part of the image in figures 4B and 4C are acquired from the rf segment on the most proximal side (i.e., closest to the heart) on the image while the bottom part corresponds to the most distal side on the image. In normal mice, the wall velocity propagated from the proximal to the distal side along the abdominal aortic wall (Fig. 3A-3D and 4B), which was translated as *regional* PW propagation along the aortic wall. However, in CaCl₂ mice, multiple waves were initiated from several regions (i.e., most likely initiated at the various calcified, i.e., stiffer, regions within the aortic wall) (Figs. 3E-3H and 4C).

Figures 6A-6D show four examples of wave velocity measurements in normal mice. The distance of the aortic wall segment from the proximal edge of the full-view B-mode is plotted as a function of the time of maximum wall velocity occurrence. The regression fit was computed for each case. The slope of the regression fit (i.e., *regional* PWV), correlation coefficient and Young's modulus were also calculated for all normal aortas (Table 1). The PWV was equal to 2.60 ± 0.57 m/s ($r^2 = 0.82 \pm 0.07$, $n = 12$).

The inner diameter and wall thickness of the abdominal aorta were measured using a standard B-mode method (Table 1). The average wall thickness was found equal to 0.13 ± 0.01 mm. Because the wall thickness was very small and close to the resolution limits of the system used, the average value for the Young's modulus calculation was used in order to avoid dispersion caused by the measurement variance. The average Young's modulus of the aorta was found equal to 50.9 ± 20.0 kPa ($n = 12$).

Figures 6E-6H depict the wave velocity measurements in four examples of four separate CaCl₂ aortas. The results were evaluated (Table 2) and compared to those computed in normal mice. As is shown in table 3, the inner diameter of the normal and CaCl₂ aortas were equal to 6.6 ± 2.4 mm and 0.87 ± 0.11 mm ($p = 0.42$). The *regional* PWV's were 2.60 ± 0.57 m/s and 2.96 ± 0.90 m/s ($p = 0.42$) while the correlation coefficients (r^2) were 0.82 ± 0.07 and 0.51 ± 0.22 ($p < 0.01$). The maximal velocities were 6.6 ± 2.4 m/s and 8.4 ± 3.2 m/s ($p = 0.29$). There was no statistically-significant difference between the velocities measured in the normal and the CaCl₂ mouse model. The correlation coefficients of linear regression established statistical significance between the two groups ($p < 0.01$). The average correlation coefficient of normal mice was significantly larger than that of CaCl₂ mice ($p < 0.01$) (Fig. 6I).

Measurements in two different segments were obtained on the rf lines at 3.6 mm and 7.2 mm from the proximal side of the PWI image. The M-mode of the wall velocity during one cardiac cycle, from one peak of the R-wave to the next, of the segment acquired from 7.2 mm from the proximal side of the full image (Fig. 7A). The wall velocity transition pattern of the CaCl₂ mice was compared to that of normal mice along the time course.

The blue and red traces in figures 5B and 5C represent the variation acquired over the entire cardiac cycle from two separate segments 3.6 mm apart (Fig. 5A). Those values were

TABLE 1. PWV, correlation coefficient, inner diameter measurements and elastic modulus calculations in all wild-type mice scanned ($n = 12$).

Mouse	PWV (m/s)	Correlation coefficient (r^2)	Inner diameter (mm)	E (kPa)
Normal 1	2.26	0.92	0.91	37.82
Normal 2	3.51	0.84	0.85	85.35
Normal 3	3.48	0.77	0.79	78.01
Normal 4	2.68	0.87	1.12	65.59
Normal 5	2.58	0.75	0.89	48.26
Normal 6	1.44	0.93	0.96	16.12
Normal 7	2.42	0.80	0.78	37.37
Normal 8	2.40	0.83	0.92	43.14
Normal 9	2.47	0.79	0.87	43.38
Normal 10	2.88	0.79	0.89	60.10
Normal 11	2.19	0.92	0.83	32.36
Normal 12	2.93	0.68	0.91	63.54
Average	2.60 ± 0.57	0.82 ± 0.06	0.89 ± 0.089	50.92 ± 20.03

traced from one peak of the R-wave to the next. Those traces acquired from normal mice (figure 5B) were compared to those acquired from CaCl_2 mice (Fig. 5C).

Histopathological section of the abdominal aorta of normal mice by H&E staining showed intact smooth muscle cells and elastic lamellae (Fig. 8A). In CaCl_2 mouse aortas, the smooth elastic lamellae were irregular, ruptured, and fragmented (Figs. 8B and 8C). Calcifications were conspicuous and smooth muscle cells were decreased in number, with abnormal morphological features, including high depositions of calcium.

DISCUSSION

PWV has been widely used to detect the progression of various diseases.^{11, 14, 44, 45} The noninvasive evaluation of *regional* PWV along the aortic wall is thought to be a long-term goal in clinical diagnosis. Ultrasonography is an easily accessible and sophisticated non-invasive technique that has been widely used in daily clinical diagnosis. However, because of the limitations in temporal and spatial resolutions of conventional ultrasonography, imaging of the *regional* PWV at standard, real-time echocardiography frame rates has been deemed fundamentally impossible. The standardized method to measure PWV is to perform two separate pressure measurements at two different sites, typically the common carotid artery and the femoral artery. This method is based on several assumptions including that the vessel wall between those two sites is entirely uniform and linear, which do not hold, especially in the case of an aorta affected by disease, i.e. localized plaques or aneurysms.²⁹ We recently developed a method for capturing the rf signals at a frame rate of 8 kHz.^{32, 35} Our technique can track and image the PW during propagation with a submillimeter resolution so that it is capable of capturing the displacement amount of the very thin (of 0.1 mm thickness) aortic wall itself (not the lumen), with or without disease. Because of the fact that disease in-

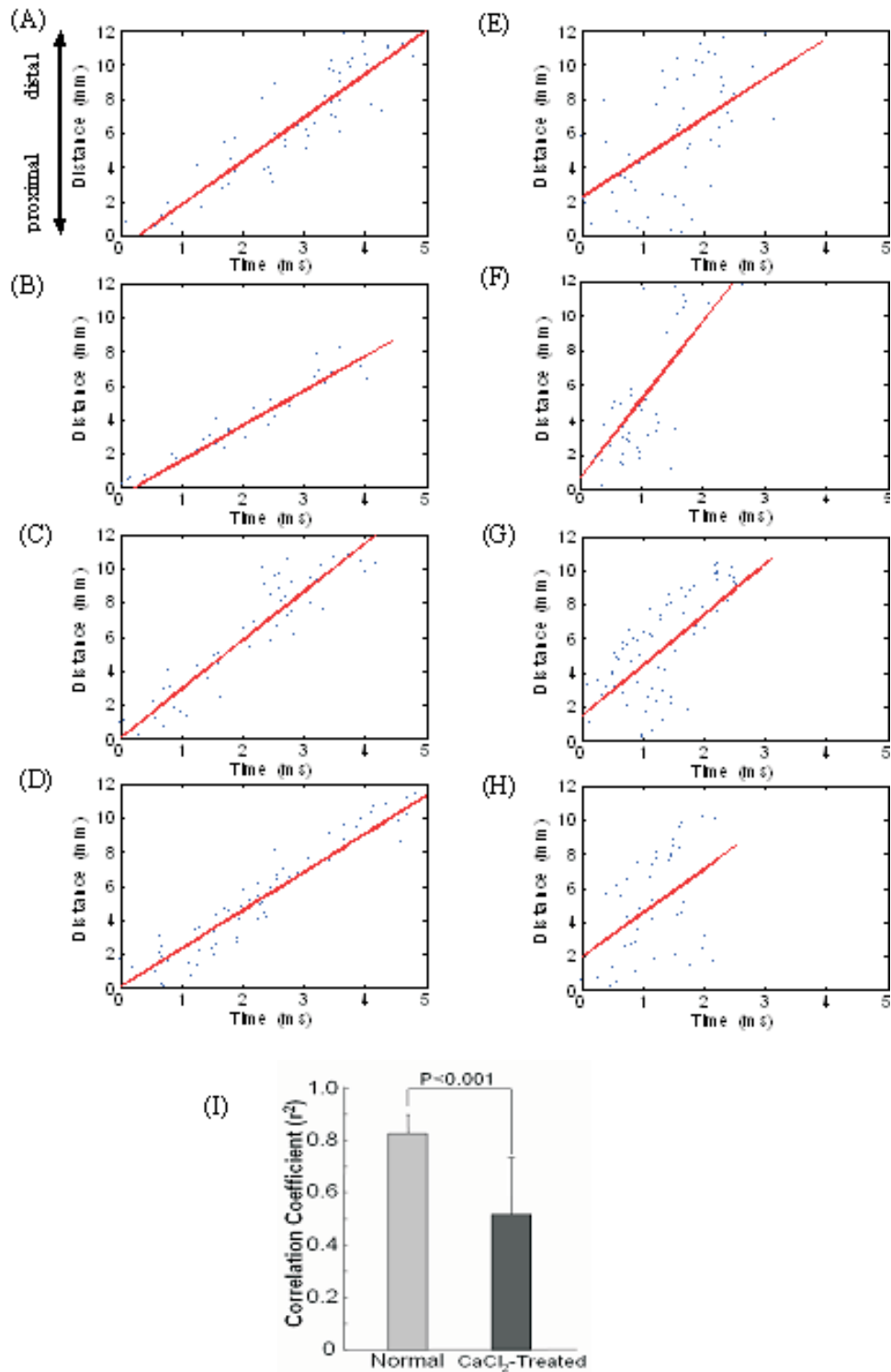


FIG. 6 A-D) Four examples of wave velocity measurements from five different normal mice. The slope of the best-fit line is the PWV in each case. E-H) Five examples of wave velocity measurements from five different CaCl_2 -model mice. The slope of the best-fit line is the PWV in each case. I) Statistical analysis of the dispersion around the regression fit shows statistical significance in detecting the presence of an aneurysm ($p < 0.01$).

TABLE 2. PWV, correlation coefficient and inner diameter measurements in all AAA mice scanned ($n = 5$). Elastic modulus calculations were not performed due to the low correlation coefficients associated with the PWV measurements.

	PWV (m/s)	Correlation coefficient (r^2)	Inner diameter (mm)
CaCl ₂ -treated 1	2.41	0.37	0.89
CaCl ₂ -treated 2	4.38	0.52	0.71
CaCl ₂ -treated 3	3.23	0.56	1.03
CaCl ₂ -treated 4	2.69	0.27	0.82
CaCl ₂ -treated 5	2.08	0.85	0.91
Average	2.96 ± 0.90	0.51 ± 0.22	0.87 ± 0.11

TABLE 3. Pulse-wave velocity (PWV), correlation coefficient (r^2), maximum velocity (mm/s) and inner diameter of the aortas of twelve normal ($n = 12$) and five CaCl₂-treated ($n = 5$) aortas. The maximum velocities were obtained from the velocity profiles (e.g., Figs. 5(B) and (C)) at different lateral positions of rf lines. The p value of the difference in each parameter between the normal and CaCl₂-treated aortas was also calculated from a Student's t-test. The difference of PWV, maximum velocity and inner diameter between normal and CaCl₂-treated mice are not statistically significant ($p > 0.1$), while r^2 shows the significant difference ($p < 0.01$) in these two groups.

	PWV (m/s)	Correlation coefficient (r^2)	Maximum velocity (mm/s)	Inner diameter (mm)
Normal ($n = 12$)	2.60 ± 0.57	0.82 ± 0.06	6.6 ± 2.4	0.89 ± 0.09
CaCl ₂ ($n = 5$)	2.96 ± 0.90	0.51 ± 0.22	8.4 ± 3.2	0.87 ± 0.11
p value	0.42	<0.01	0.29	0.42

herently causes regional vascular nonuniformities, we believe that this new method can be proven more accurate since the *regional* PWV is measured. Also, as mentioned in the introduction, various investigators have indicated that imaging of the PW and detecting the *regional* PWV in the aorta may contribute to a future screening test and reduction of the overall morbidity and mortality from AAA's and other cardiovascular diseases.^{26, 28, 30, 31}

The transition of the wall velocity was qualitatively evaluated using the resulting color-coded ciné-loop (Fig. 3). Because of the nature of our study to map and evaluate wall velocity, we used the peak-peak method instead of the conventional foot-foot method. In normal mice, the *regional* PW propagates from the proximal to the distal side at constant speed, whereas in the CaCl₂ aortas, the wave was reflected at multiple locations due to the higher nonuniformities verified with histology (Fig. 8). The PWV estimated in the normal mouse aorta in this study (2.60 ± 0.57 m/s) was in agreement with previous reports using catheter insertion measuring the luminal blood flow (2.6 - 4.4 m/s).^{46, 47} Our results are also within the range of the PWV in the mouse aorta estimated from pulsed Doppler techniques (2.2 - 8.5 m/s).²² However, in CaCl₂ mice, the correlation coefficient of the best fit line was very low, which supported the results of the above visualization analysis, which can be explained by a nonuniform calcification of the aortic wall (Fig. 8).

Because the PWV measured by our technique was relatively high, the original acquiring frame rate was essential. The wall velocity shown in this paper was obtained from the incre-

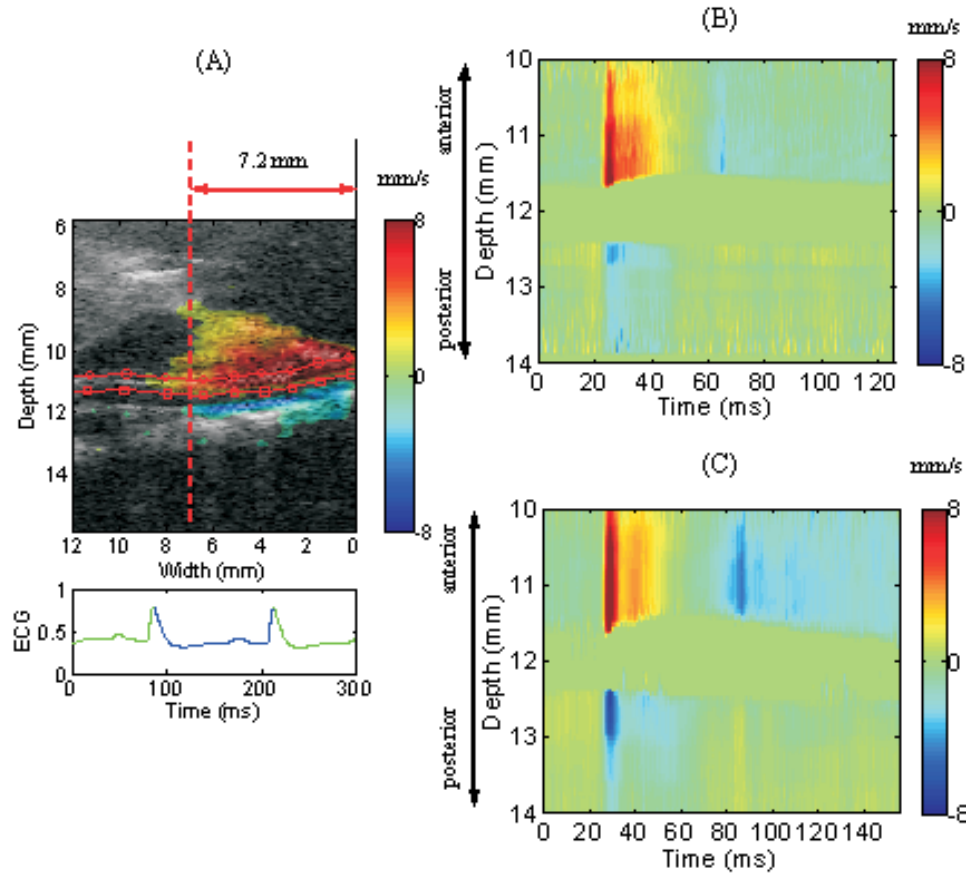


FIG. 7 A) PWI map and designation of the location monitored with time in 2D spatiotemporal maps B) normal and C) CaCl₂-model murine. Example M-mode displacement images of B) normal and C) CaCl₂-model murine were acquired from 7.2 mm from the proximal side of the 2D full image.

mental/instantaneous displacement between successive frames multiplied by the frame rate. However, both the forward (highest wall velocity peak) and the reflection (second highest wall velocity peak) wave right after the forward peak can clearly be seen (Figs. 5B and 5C). We estimated displacements between consecutive rf frames, as shown in figure 2B, to maintain the effective frame rate as high as in the ultrasound acquisition (8 kHz). As is shown in table 3, the correlation coefficient (r^2) was thus deemed to be the most reliable parameter with the only high statistical significance between normal and pathological aortic states in the case of the CaCl₂ model, even when compared to standard clinical parameters such as the lumen diameter and wall thickness. This novel *regional* PW imaging technique may be capable of characterizing and imaging normal aortas and detecting vulnerability of plaque and/or aneurysm rupture.

The sonographic axial resolution of the system used was equal to 55 μm . The window shift used in our study (24 μm) was sufficiently small to preserve the high axial resolution and the *regional* PW axial resolution with this method could be similar to that of sonography (55 μm).³⁶ In this study, the beam density was equal to 12 beams/mm, equivalent to a beam spacing of about 85 μm , much higher than what has been previously reported, which was on the order of 0.01-1 beam/mm. Therefore, the lateral resolution of our wall velocity analysis was similar to the sonographic lateral resolution of 115 μm .

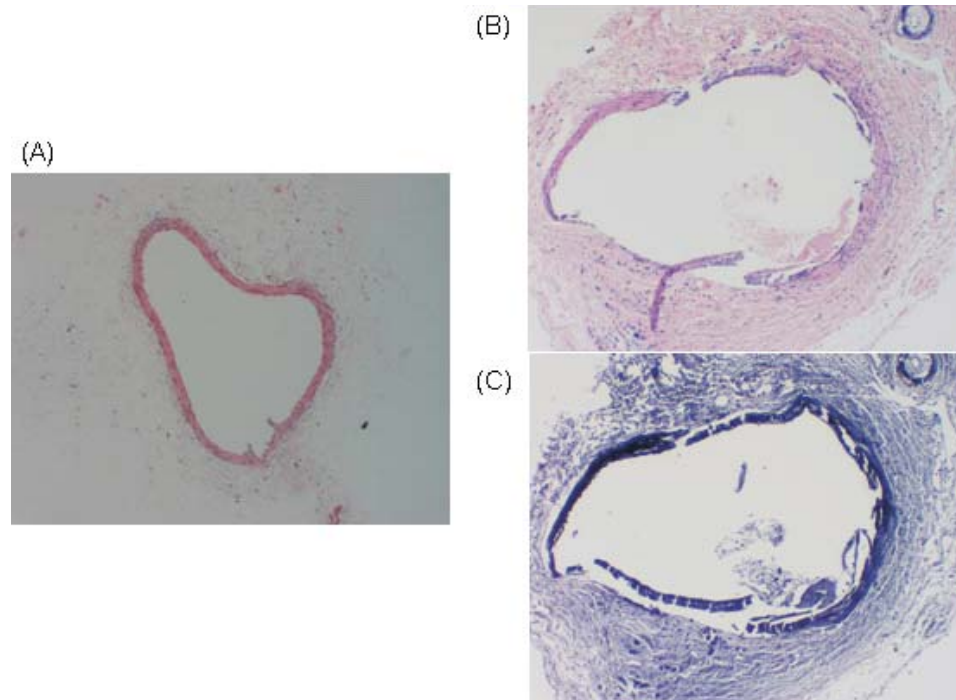


FIG. 8 A) H&E of normal aorta from a sham operation (10x), B) H&E of CaCl₂ treated aorta (10x) and C) EVG-stained (for elastin in blue) of CaCl₂ treated aorta (10x). Calcifications were conspicuous in CaCl₂ treated aortic wall, and smooth muscle cells were decreased in number, with abnormal morphological features, including depositions of calcium.

In order to scan the abdominal aorta *in vivo*, the ultrasound beam propagates through the abdominal wall, connective tissue, gastrointestinal tract, peritoneal membrane, etc. The path of the ultrasound beam is not uniform before reaching the aorta, which may result in some variability of the individual data. Variability of these measurements can be reduced by averaging values over an adequately-sized area. The linear regression was therefore acquired after averaging. The correlation coefficient in normal mice, whose aortic wall was relatively uniform, confirmed the high reliability of our PWV evaluation.

In the calculation of the Young's modulus, individual *regional* PWV, individual inner radius of the aorta, average wall thickness and fixed wall density were applied. Because the wall thickness of the murine abdominal aorta was very small (~0.1 mm) and the standard deviation of those measurements was relatively high, those values were close to the lowest limitation of our measurement accuracy. The average, rather than an individual value, was deemed more reliable for minimization of the measurement error. In normal models, the density of the wall can be substituted for the density of the blood but this estimate has limitations in disease models. The Young's modulus was derived using a previously-developed and relatively-simple theoretical model. The surrounding tissue is known to affect the elastic module of the arteries.³⁰ Because the diet of the mice before the experiment was not controlled or monitored, the amount of digesta in the tract and the amount of peristalsis may have varied depending on the mice, which may have dispersed our data.

Although the longitudinal image of the aorta with the largest diameter was always acquired, the location of the aorta and the angle of the transducer to the aorta were not always the same. This could be because of the variable extent of permeability of the tissue or organs found between the transducer and the aorta. A scan with the longest view of the aorta on the

screen was therefore displayed. The aortas in most mice could be displayed between 8 mm and 12 mm in length, which was 2/3 to 1 in ratio of the maximal scanning ability (Fig. 6).

Figure 7B and 7C show the constriction and dilation patterns of the aorta as a function of time. The dilation speed was composed of two components, early dilation and later dilation. The aorta dilates quickly immediately following the *regional* PW stimulation (i.e., the early dilation component), and then dilates at a slower speed (i.e., the later dilation component). The pressure wave in the aorta is the sum of the initial pressure wave (i.e., the pressure wave generated by the left ventricle in systole) and pressure wave reflected back from the periphery.^{41, 48, 49} The early dilation component corresponds to the initial pressure wave while the late one corresponds to the pressure wave due to reflection.

The PWV was calculated from the slope of the regression fit through several wall velocity samples within 1 cm of the mouse aorta. It is deemed that the PWV results are less dependent on the position of the measurement because the linear regression method can smooth any effects of noise and provide average results using all the high-resolution data available. More importantly, uniform propagation of the PW in 12 normal aortas has been observed and reported in this paper while these data have been acquired over thousands of cardiac cycles, each one over seven minutes. In addition, several authors have studied the dynamics of the aorta using MRI, which inherently uses ECG-gating (i.e., over multiple cardiac cycles) to perform these measurements.^{50, 51} Therefore, both the existent literature and our experience indicate that retrospective ECG gating does not have a significant effect on the measurements.

Finally, this method can be used at both low and high ultrasound frequencies. The depth and the size of the field of view will change proportionally. The same technique may be applied for detection of disease in conjunction with ultrasound systems used in a clinical setting, as we have recently shown.⁵²

CONCLUSION

This study demonstrated a state-of-the-art *regional* PW imaging technique that depicted PW propagation *in vivo* along the abdominal aortic wall of mice using extremely high frame rates. The high axial resolution (55 μm) enabled motion estimation of the murine abdominal aortic wall at high precision. In normal mice, the *regional* PW propagated from the proximal to the distal side at a constant speed, whereas in CaCl_2 aortas, the wave was reflected at multiple locations. Although there was no statistical difference in the *regional* PWV between normal and CaCl_2 -treated aortas, the correlation coefficient was significantly lower in the CaCl_2 -treated aortas. This technique allows noninvasive assessment of normal and pathological aortas *in vivo*. In future applications, it may thus contribute to the detection of early-stages vascular degeneration.

ACKNOWLEDGMENTS

This work was supported in part by the American Heart Association under Grant 0435444AT and by a grant from the associate trustees of St. Luke's-Roosevelt Hospital. The authors are grateful to Shunichi Homma, M.D., Department of Medicine, Columbia University, for kindly allowing access to the ultrasound system used for the experiments. The authors appreciate Charles C. Marboe, M.D., Department of Pathology, Columbia University, for his help in the assessment of the histopathology data.

REFERENCES

1. Aggoun Y, Szezepanski I, Bonnet D. Noninvasive assessment of arterial stiffness and risk of atherosclerotic events in children, *Pediatr Res* 58, 173-178 (2005).
2. Sutton-Tyrrell K, Najjar SS, Boudreau RM, et al. Elevated aortic pulse wave velocity, a marker of arterial stiffness, predicts cardiovascular events in well-functioning older adults, *Circulation* 111, 3384-3390 (2005).
3. Sato H, Hayashi J, Harashima K, Shimazu H, Kitamoto K. A population-based study of arterial stiffness index in relation to cardiovascular risk factors, *J Atheroscler Thromb* 12, 175-180 (2005).
4. Laurent S, Boutouyrie P, Asmar R, Gautier I, et al. Aortic stiffness is an independent predictor of all-cause and cardiovascular mortality in hypertensive patients, *Hypertension* 37, 1236-1241 (2001).
5. Boutouyrie P, Tropeano AI, Asmar R, et al. Aortic stiffness is an independent predictor of primary coronary events in hypertensive patients - a longitudinal study, *Hypertension* 39, 10-15 (2002).
6. Lehmann ED, Hopkins KD, Rawesh A, et al. Relation between number of cardiovascular risk factors/events and noninvasive Doppler ultrasound assessments of aortic compliance, *Hypertension* 32, 565-569 (1998).
7. Marque V, Kieffer P, Gayraud B, et al. Aortic wall mechanics and composition in a transgenic mouse model of Marfan syndrome, *Arterioscler Thromb Vasc Biol* 21, 1184-1189 (2001).
8. Steptoe A, Smulyan H, Gribbin B. Pulse-wave velocity and blood-pressure change - calibration and applications, *Psychophysiology* 13, 488-493 (1976).
9. Pruet JD, Bourland JD, Geddes LA. Measurement of pulse-wave velocity using a beat-sampling technique, *Ann Biomed Eng* 16, 341-347 (1988).
10. Nagai Y, Fleg JL, Kemper MK, et al. Carotid arterial stiffness as a surrogate for aortic stiffness: relationship between carotid artery pressure-strain elastic modulus and aortic pulse wave velocity, *Ultrasound Med Biol* 25, 181-188 (1999).
11. Farrar DJ, Bond MG, Sawyer JK, Green HD. Pulse-wave velocity and morphological-changes associated with early atherosclerosis progression in the aortas of cynomolgus monkeys, *Cardiovasc Res* 18, 107-118 (1984).
12. Farrar DJ, Bond MG, Riley WA, Sawyer JK. Anatomic correlates of aortic pulse-wave velocity and carotid-artery elasticity during atherosclerosis progression and regression in monkeys, *Circulation* 83, 1754-1763 (1991).
13. O'Rourke MF, Staessen JA, Vlachopoulos C, Duprez D, Plante GE. Clinical applications of arterial stiffness; definitions and reference values, *Am J Hypertens* 15, 426-444 (2002).
14. Cruickshank K, Riste L, Anderson SG, et al. Aortic pulse-wave velocity and its relationship to mortality in diabetes and glucose intolerance - An integrated index of vascular function?, *Circulation* 106, 2085-2090 (2002).
15. Blacher J, Guerin AP, Pannier B, et al. Impact of aortic stiffness on survival in end-stage renal disease, *Circulation* 99, 2434-2439 (1999).
16. Macsweeney STR, Young G, Greenhalgh RM, Powell JT. Mechanical-properties of the aneurysmal aorta, *Br J Surg* 79, 1281-1284 (1992).
17. Long A, Rouet L, Bissery A, Goeau-Brissoniere O, Sapoval M. Aortic compliance in healthy subjects: Evaluation of tissue Doppler imaging, *Ultrasound Med Biol* 30, 753-759 (2004).
18. Long A, Rouet L, Bissery A, et al. Compliance of abdominal aortic aneurysms evaluated by tissue Doppler imaging: Correlation with aneurysm size, *J Vasc Surg* 42, 18-26 (2005).
19. Jadhav UM, Kadam NN. Non-invasive assessment of arterial stiffness by pulse-wave velocity correlates with endothelial dysfunction, *Indian Heart J* 57, 226-32 (2005).
20. Truijers M, Pol JA, SchultzeKool LJ, et al. Wall stress analysis in small asymptomatic, symptomatic and ruptured abdominal aortic aneurysms, *Eur J Vasc Endovasc Surg* 33, 401-407 (2007).
21. Vande Geest JP, Wang DHJ, Wisniewski SR, Makaroun MS, Vorp DA. Towards a noninvasive method for determination of patient-specific wall strength distribution in abdominal aortic aneurysms, *Ann Biomed Eng* 34, 1098-1106 (2006).
22. Hartley CJ, Taffet GE, Michael LH, Pham TT, Entman ML. Noninvasive determination of pulse-wave velocity in mice, *Am J Physiol-Heart Circul Physiol* 42, H494-H500 (1997).
23. Brands PJ, Willigers JM, Ledoux LAF, Reneman RS, Hoeks APG. A noninvasive method to estimate pulse wave velocity in arteries locally by means of ultrasound, *Ultrasound Med Biol* 24, 1325-1335 (1998).

24. Meinders JM, Kornet L, Brands PJ, Hoeks APG. Assessment of local pulse wave velocity in arteries using 2D distension waveforms, *Ultrasonic Imaging* 23, 199-215 (2001).
25. Eriksson A, Greiff E, Loupas T, Persson M, Pesque P. Arterial pulse wave velocity with tissue Doppler imaging, *Ultrasound Med Biol* 28, 571-580 (2002).
26. Zhang XM, Greenleaf JF. Noninvasive generation and measurement of propagating waves in arterial walls, *J Acoust Soc Am* 119, 1238-1243 (2006).
27. Rabben SI, Baerum S, Sorhus V, Torp H. Ultrasound-based vessel wall tracking: an auto-correlation technique with RF center frequency estimation, *Ultrasound Med Biol* 28, 507-17 (2002).
28. Xu JP. Do we need a better approach for measuring pulse-wave velocity?, *Ultrasound Med Biol* 29, 1373-1373 (2003).
29. Karamanoglu M. Errors in estimating propagation distances in pulse wave velocity, *Hypertension* 41, E8-E8 (2003).
30. Zhang XM, Greenleaf JF. The stiffening of arteries by the tissue-mimicking gelatin, *IEEE Trans Ultrason Ferroelectr Freq Contr* 53, 1534-1539 (2006).
31. Zhang XM, Greenleaf JF. Measurement of wave velocity in arterial walls with ultrasound transducers, *Ultrasound Med Biol* 32, 1655-1660 (2006).
32. Pernot M, Konofagou EE. Electromechanical imaging of the myocardium at normal and pathological states, in *Proc IEEE Ultrasonics Symp*, pp. 1091-1094 (2005).
33. Cherin E, Williams R, Needles A, et al. Ultrahigh frame rate retrospective ultrasound microimaging and blood flow visualization in mice in vivo, *Ultrasound Med Biol* 32, 683-691 (2006).
34. Liu JH, Jeng GS, Wu TK, Li PC. ECG triggering and gating for ultrasonic small animal imaging, *IEEE Trans Ultrason Ferroelectr Freq Contr* 53, 1590-1596 (2006).
35. Pernot M, Fujikura K, Fung-Kee-Fung SD, Konofagou EE. ECG-gated, mechanical and electromechanical wave imaging of cardiovascular tissues in vivo, *Ultrasound Med Biol* 33, 1075-1085 (2007).
36. Luo J, Fujikura K, Homma S, Konofagou EE. Myocardial elastography at both high temporal and spatial resolution for the detection of infarcts, *Ultrasound Med Biol* 33, 1206-1223 (2007).
37. Williams R, Needles A, Cherin E, et al. Noninvasive ultrasonic measurement of regional and local pulse-wave velocity in mice, *Ultrasound Med Biol* 33, 1368-1375 (2007).
38. Ophir J, Cespedes I, Ponnekanti H, Yazdi Y, Li X. Elastography - a quantitative method for imaging the elasticity of biological tissues, *Ultrasonic Imaging* 13, 111-134 (1991).
39. Viola F, Walker WF. A comparison of the performance of time-delay estimators in medical ultrasound, *IEEE Trans Ultrason Ferroelectr Freq Contr* 50, 392-401 (2003).
40. Landau LD, Lifshitz EM, Kosevich AM, Pitaevskii LP. *Theory of Elasticity*, 3rd English Ed. (Pergamon Press, Oxford, 1986).
41. Nichols WW, O'Rourke MF, McDonald DA. *McDonald's Blood Flow in Arteries: Theoretical, Experimental and Clinical Principles*, 5th Ed. (Hodder Arnold, New York, 2005).
42. Chiou AC, Chiu B, Pearce WH. Murine aortic aneurysm produced by periarterial application of calcium chloride, *J Surg Res* 99, 371-376 (2001).
43. Daugherty A, Cassis LA. Mouse models of abdominal aortic aneurysms, *Arterioscler Thromb Vasc Biol* 24, 429-434 (2004).
44. Woolam GL, Schnur PL, Vallbona C, Hoff HE. Pulse wave velocity as an early indicator of atherosclerosis in diabetic subjects, *Circulation* 25, 533-539 (1962).
45. Blacher J, Safar ME, Guerin AP, et al. Aortic pulse wave velocity index and mortality in end-stage renal disease, *Kidney Int* 63, 1852-1860 (2003).
46. Wang YX, Halks-Miller M, Vergona R, et al. Increased aortic stiffness assessed by pulse wave velocity in apolipoprotein E-deficient mice, *Am J Physiol-Heart Circul Physiol* 278, H428-H434 (2000).
47. Segers P, Georgakopoulos D, Afanasyeva M, et al. Conductance catheter-based assessment of arterial input impedance, arterial function, and ventricular-vascular interaction in mice, *Am J Physiol-Heart Circul Physiol* 288, H1157-H1164 (2005).
48. Hartley CJ, Reddy AK, Madala S, et al. Noninvasive ultrasonic measurement of arterial wall motion in mice, *Am J Physiol-Heart Circul Physiol* 287, H1426-H1432 (2004).

49. Brands PJ, Hoeks APG, Rutten MCM, Reneman RS. A noninvasive method to estimate arterial impedance by means of assessment of local diameter change and the local center-line blood flow velocity using ultrasound, *Ultrasound Med Biol* 22, 895-905 (1996).
50. Naganawa S, Ishiguchi T, Ishigaki T, et al. Real-time interactive MR imaging system: sequence optimization, and basic and clinical evaluations, *Radiation Med* 18, 71-9 (2000).
51. Pereles FS, McCarthy RM, Baskaran V, et al. Thoracic aortic dissection and aneurysm: evaluation with nonenhanced true FISP MR angiography in less than 4 minutes, *Radiology* 223, 270-274 (2002).
52. Wang S, Lee W-N, Luo J, Konofagou EE. An ECG gated clinical ultrasound system for high frame-rate cardiovascular imaging, in *Proc IEEE Ultrason Symp* (2007, in press).